

The Nature Of Radio Continuum Emission At Very Low Metallicity: *VLA* Observations of I Zw 18

John M. Cannon and Fabian Walter

Max-Planck-Institut für Astronomie, Königstuhl 17, D-69117 Heidelberg, Germany

cannon@mpia.de; walter@mpia.de

Evan D. Skillman

*Department of Astronomy, University of Minnesota,
116 Church St. S.E., Minneapolis, MN 55455, USA*

skillman@astro.umn.edu

Liese van Zee

*Department of Astronomy, Indiana University,
727 East Third Street, Bloomington, IN 47405, USA*

vanzee@astro.indiana.edu

ABSTRACT

We present the first resolved study of the radio continuum properties of I Zw 18, the dwarf galaxy with the lowest known nebular metal abundance in the local universe. New *Very Large Array* radio continuum images at 20 and 3.6 cm are compared to various *Hubble Space Telescope* images, and we find a striking morphological similarity between high resolution $H\alpha$ and short wavelength radio continuum emission, especially in the $H\alpha$ shell in the northwest region. We separate thermal and nonthermal components of the emission, and find a large synchrotron halo surrounding the galaxy. Comparison between $H\alpha$ and X-band fluxes suggests that the emission at 3.6 cm is dominated by thermal processes; an additional synchrotron component dominates the flux at 20 cm and produces a modest fraction of the detected flux at 3.6 cm. The fluxes of three of the four major emission peaks show a mix of thermal and nonthermal processes, while one shows a nearly flat spectral index. The strong synchrotron component argues for active star formation throughout the disk for at least the last ~ 30 Myr.

These sensitive observations provide a new, detailed view of the nature of radio continuum emission in the very low metallicity interstellar medium. Comparing with the literature, the role of metallicity in the evolution of radio continuum emission seems to be secondary to other factors such as recent star formation history and the presence or absence of outflows from star formation regions.

Subject headings: galaxies: evolution — galaxies: dwarf — galaxies: individual (IZw 18) — radio continuum: galaxies

1. Introduction

With the lowest nebular metallicity known in the local universe [(O/H) \sim 0.02 (O/H) $_{\odot}$; Skillman & Kennicutt 1993], IZw 18 plays a key role in the study of galaxy evolution. Understanding the nature of the star-forming fragments predicted at high redshift requires a detailed study of nearby potentially “young” galaxies. Estimates of the age of the stellar population in IZw 18 based on single-star photometry suggest an age of less than 1 Gyr (e.g., Hunter & Thronson 1995; Aloisi et al. 1999; Östlin 2000; Izotov & Thuan 2004).

An alternative probe of the unobscured, recent (\lesssim 30 Myr) star formation in a galaxy can be obtained with radio continuum observations. Three types of radio continuum emission are seen in local star-forming galaxies (see Condon 1992 for a detailed review). First, thermal free-free emission (characterized by a nearly flat spectral index, $\alpha \sim -0.1$, where $S_{\nu} \sim \nu^{\alpha}$) is proportional to the total Lyman continuum flux and hence can be used as an accurate star formation rate estimator. Second, nonthermal synchrotron emission, produced in supernovae (SNe) explosions and remnants, shows a more negative spectral index ($-1.2 \lesssim \alpha \lesssim -0.4$). Finally, free-free absorption can occur in young, dense, heavily-embedded clusters that show an inverted spectrum ($\alpha > 0.0$; Turner et al. 1998, Kobulnicky & Johnson 1999, Johnson & Kobulnicky 2003). Distinguishing between these emission mechanisms allows one to constrain the ages of the emitting components: inverted sources are very young (ages $\sim 10^5 - 10^6$ yr; Johnson et al. 2001); thermal regions have ages comparable to those of H II regions (\lesssim 10 Myr); synchrotron radiation dominates in regions older than this.

Considering the amount of observational attention that IZw 18 has received, it is somewhat surprising that no detailed investigation of its radio continuum properties exists in the literature. There have been two previously published radio continuum detections, but both have been extracted from spectral line observations (Lequeux & Viallefond 1980; van Zee et al. 1998). In order to study the nature of radio continuum emission at the lowest avail-

able nebular metallicity, we have obtained sensitive *Very Large Array* (*VLA*)¹ observations of IZw 18. We compare these data to *Hubble Space Telescope* (*HST*)² images of the stellar and nebular emission. Throughout this paper, we adopt a distance of 12.6 Mpc for IZw 18 (Östlin 2000); however, most of our results (spectral indices, comparison to *HST* imaging) do not require a tightly-constrained distance estimate.

2. Observations and Data Reduction

2.1. *VLA* Radio Continuum Data

VLA radio continuum imaging was obtained using the A, B, and C arrays on 2003, August 3, and 2004, January 20 and April 20 (total on-source integration time = 15.1 hours) for program AC681. All reductions were performed using the Astronomical Image Processing System (AIPS) package. First, interference and bad data were removed. Flux, gain and phase calibrations were then applied, derived from observations of 1331+305 (3c286; primary calibrator) and 0921+622 (secondary calibrator). The L-band (20 cm) and X-band (3.6 cm) observations were obtained in two arrays, and these *u-v* databases were concatenated. The calibrated *u-v* data were then imaged and cleaned to produce matched-beam images at each frequency that balanced resolution and sensitivity. We analyze a set of “high” resolution (L-band: beam = $2.18'' \times 2.01''$, rms = $11.6 \mu\text{Jy beam}^{-1}$; X-band: beam = $2.17'' \times 2.07''$, rms = $7.4 \mu\text{Jy beam}^{-1}$) and a set of “low” resolution (beam = $4.5''$, L-band rms = $19 \mu\text{Jy beam}^{-1}$, X-band rms = $12 \mu\text{Jy beam}^{-1}$) images.

2.2. *HST* Imaging

We compare our radio observations to archival *HST* observations of IZw 18 from programs GO-5434 (P.I. Dufour), GO-6536 (P.I. Skillman), and GO-9400 (P.I. Thuan). The detailed handling of the data from programs 6536 and 5434 are presented in Cannon et al. (2002). We use the same narrowband H α image presented in that work for analysis here [total H α flux = $(3.26 \pm 0.3) \times 10^{-13} \text{ erg s}^{-1} \text{ cm}^{-2}$, implying a current star formation rate of

¹The National Radio Astronomy Observatory is a facility of the National Science Foundation operated under cooperative agreement by Associated Universities, Inc.

²Based on observations with the NASA/ESA Hubble Space Telescope, obtained at the Space Telescope Science Institute, which is operated by the Association of Universities for Research in Astronomy, Inc. under NASA contract No. NAS5-26555.

$\sim 0.05 M_{\odot} \text{ yr}^{-1}$ (Kennicutt et al. 1994)]. From program 9400, we use an *HST*/ACS F555W image for comparison with the stellar continuum. Based on the positions of *HST* Guide Stars in the ACS field and the agreement of the radio and $\text{H}\alpha$ peaks, we conservatively estimate the uncertainty in the coordinate solution to be better than $0.5''$ rms.

3. The Nature of Radio Continuum Emission

3.1. Global Flux Measurements

In Figure 1 we present the low-resolution images overlaid with contours at various levels. We measure global flux densities (by integrating continuous emission surrounding the galaxy after blanking at the 3σ level) at L- and X-bands of 1.79 ± 0.18 mJy and 0.78 ± 0.08 mJy, respectively, corresponding to a global spectral index of -0.46 ± 0.06 (see Table 1). The continuum emission is more spatially extended at 20 cm than at 3.6 cm (although the latter data are significantly more sensitive); indeed, emission above the 3σ level is detected out to $\sim 12''$ (deconvolved) northwest of the emission peak at L-band (corresponding to a linear distance of ~ 730 pc at the adopted distance), but only to $\sim 7.5''$ at X-band. As argued in the next section, this is the result of a synchrotron halo surrounding the system.

3.2. Thermal vs. Nonthermal Decomposition

Since the thermal radio continuum luminosity is proportional to the total photoionization rate, there exists a well-defined relation between radio continuum luminosity and other direct star formation rate indicators (e.g., $\text{H}\alpha$ emission). In systems with little extinction in the optical, this relation can be used to estimate the expected thermal fraction of detected radio continuum emission. In I Zw 18, the low detected extinctions ($A_V \lesssim 0.5$ mag.; see Cannon et al. 2002) imply that $\text{H}\alpha$ provides a nearly complete census of the ongoing star formation.

We can estimate the expected thermal components at each frequency using the relations presented in Caplan & Deharveng (1986). For a purely thermal radio continuum source in the absence of extinction, the $\text{H}\alpha$ flux and the flux density at a given frequency are related via:

$$\frac{j_{\text{H}\alpha}}{j_{\nu}} = \frac{(8.67 \times 10^{-9})(T)^{-0.44}}{(10.811 + 1.5 \cdot \ln(T) - \ln(\nu))} \quad (1)$$

where $j_{H\alpha}$ is the flux at $H\alpha$ in $\text{erg s}^{-1} \text{cm}^{-2}$, j_ν is the flux density at the given frequency in Jy, T is the electron temperature in units of 10^4 K, and ν is the observed frequency in GHz. We adopt an intermediate electron temperature from Skillman & Kennicutt (1993) of 18500 K for the entire galaxy. Using the global $H\alpha$ flux measured from the *HST* image (see Table 1), we expect flux densities of 0.47 mJy at X-band and 0.56 mJy at L-band. Comparison with the measured X-band value of 0.78 mJy suggests that more than half of the 3.6 cm emission is thermal; conversely, only $\sim 30\%$ of the emission at L-band is expected to be thermal.

Given this expected value for thermal emission at 20 cm, $> 70\%$ of the detected emission can be attributed to a synchrotron component. If this emission has a characteristic synchrotron spectral index ($\alpha = -0.8$), then this implies a synchrotron contribution to the detected flux at X-band of 0.29 mJy. This value can be compared with the difference between total and (predicted) thermal fluxes, 0.31 mJy; the agreement suggests that such a synchrotron component fits the data quite well.

3.3. Properties of Individual Radio Emission Peaks

We present higher resolution images of the radio continuum emission from IZw 18 in Figures 2 and 3, as well as overlays of the emission on *HST* $H\alpha$ and V-band images. We resolve the emission into 4 distinct peaks at this resolution. Examining these images, there is a striking correlation between $H\alpha$ and radio continuum emission at this sensitivity level; in all areas of high surface brightness $H\alpha$ emission, strong radio continuum emission is prevalent. Note also that the radio continuum emission closely follows the diffuse $H\alpha$ shell morphology in the northwest region.

The total flux densities of the individual peaks were measured using identical apertures the size of the beam or larger, centered on the peaks in the X-band image (see Figure 2 and Table 1). The individual radio continuum peaks are found to have a mix of thermal and nonthermal spectral indices. Three of the sources (IZw 18 SE, NW-A, NW-C) have spectral indices $\alpha \sim -0.27$, implying a mix of thermal and nonthermal components. IZw 18 NW-B, however, is consistent with nearly purely thermal emission ($\alpha = -0.04 \pm 0.06$).

Sources IZw 18 SE and NW-A are clearly associated with collections of the high surface brightness H II regions of the galaxy. The high (aperture integrated) $H\alpha$ equivalent widths found in Cannon et al. (2002) imply strong active star formation, while their nonthermal radio continua suggest that the areas are also rich in massive star feedback via SNe explosions and remnants. This suggests that the star formation intensity was strong ~ 20 -30 Myr ago, as well as at the present epoch. This is in good agreement with the results of resolved stellar

population analysis, where recent investigations have found a star formation rate that was elevated during the last 10-100 Myr compared to that at present (Aloisi et al. 1999; Östlin 2000; Izotov & Thuan 2004).

4. Discussion and Conclusions

The nature of radio continuum emission at very low metallicities is only beginning to be explored. Comparing our results with those on the second-most metal poor galaxy known, SBS 0335–052 (Hunt et al. 2004), we find that both systems have a mix of nonthermal and thermal components, indicative of active massive star formation over the last ~ 30 Myr. However, the radio spectrum of SBS 0335–052 has a thermal component that manifests itself in considerable absorption at L-band and a radio turnover between 1.4 and 4.8 GHz. While the present dataset has fewer frequencies, we would be sensitive to a similar spectral turnover in IZw 18 (as this would result in positive, rather than negative, spectral indices between 3.6 and 20 cm).

The differences in the radio continuum properties of IZw 18 and SBS 0335–052 are most easily explained as the results of the more vigorous star formation event that is underway in the latter. IZw 18 appears to be undergoing star formation in discrete stellar clusters and H II regions [see Table 1 for $H\alpha$ luminosities of the radio emission peaks studied here, and Cannon et al. (2002) for those of other clusters], and infrared imaging (e.g., Östlin 2000; Östlin & Mouchine 2005) does not suggest embedded regions that would be able to give rise to “super star clusters” (SSCs; see O’Connell 2004 for a recent review of SSC properties). SBS 0335–052, on the other hand, hosts multiple SSCs (Thuan et al. 1997) and regions of exceptionally high extinction and embedded star formation for a very metal poor galaxy (Hunt et al. 2001; Plante & Sauvage 2002). Given that complex (and often inverted) spectral indices typically arise from such regions (Turner et al. 1998; Kobulnicky & Johnson 1999; Johnson & Kobulnicky 2003), it is perhaps not surprising that the radio spectra of IZw 18 and SBS 0335–052 appear to differ.

To summarize, we have detected thermal and nonthermal emission in IZw 18, including a synchrotron halo. This low-metallicity, low-dust system shows a radio continuum spectrum between 20 and 3.6 cm that is typical of star-forming dwarf galaxies; however, the radio properties differ markedly from those found in the second most metal-poor galaxy, SBS 0335–052. Although the sample is small, the variety of radio continua found at very low metallicities suggests that there is not a strong metallicity dependence for the production of radio continuum emission. Indeed, it is not necessary that one should exist; thermal continua are produced by stars that have formed, while nonthermal continua are typically

the result of the evolution of massive stars. While there certainly exist differences in the way that the stars form at different metallicities, once the stars have formed, radio continuum emission appears to be ubiquitous (though complex and dependent on other factors) in massive star formation regions regardless of metallicity.

The authors would like to thank Chip Kobulnicky for helpful discussions during the planning stages of this project, and the anonymous referee for helpful comments.

REFERENCES

- Aloisi, A., Tosi, M., & Greggio, L. 1999, *AJ*, 118, 302
- Cannon, J. M., Skillman, E. D., Garnett, D. R., & Dufour, R. J. 2002, *ApJ*, 565, 931
- Caplan, J. & Deharveng, L. 1986, *A&A*, 155, 297
- Condon, J. J. 1992, *ARA&A*, 30, 575
- Hunt, L. K., Dyer, K. K., Thuan, T. X., & Ulvestad, J. S. 2004, *ApJ*, 606, 853
- Hunt, L. K., Vanzi, L., & Thuan, T. X. 2001, *A&A*, 377, 66
- Hunter, D. A. & Thronson, H. A. 1995, *ApJ*, 452, 238
- Izotov, Y. I. & Thuan, T. X. 2004, *ApJ*, 616, 768
- Johnson, K. E. & Kobulnicky, H. A. 2003, *ApJ*, 597, 923
- Johnson, K. E., Kobulnicky, H. A., Massey, P., & Conti, P. S. 2001, *ApJ*, 559, 864
- Kennicutt, R. C., Tamblyn, P., & Congdon, C. E. 1994, *ApJ*, 435, 22
- Kobulnicky, H. A. & Johnson, K. E. 1999, *ApJ*, 527, 154
- Lequeux, J. & Viallefond, F. 1980, *A&A*, 91, 269
- O’Connell, R. W. 2004, ASP Conf. Ser. 322: The formation and evolution of massive young star clusters, eds. H.J.G.L.M. Lamers, L.J. Smith & A. Nota (San Francisco: ASP), in press (astro-ph/0405038)
- Östlin, G. 2000, *ApJ*, 535, L99
- Östlin, G. & Mouchine, M. 2005, *A&A*, in press (astro-ph/0411217)
- Plante, S. & Sauvage, M. 2002, *AJ*, 124, 1995
- Skillman, E. D. & Kennicutt, R. C. 1993, *ApJ*, 411, 655
- Thuan, T. X., Izotov, Y. I., & Lipovetsky, V. A. 1997, *ApJ*, 477, 661
- Turner, J. L., Ho, P. T. P., and Beck, S. C. 1998, *AJ*, 116, 1212
- van Zee, L., Westpfahl, D., Haynes, M. P., & Salzer, J. J. 1998, *AJ*, 115, 1000

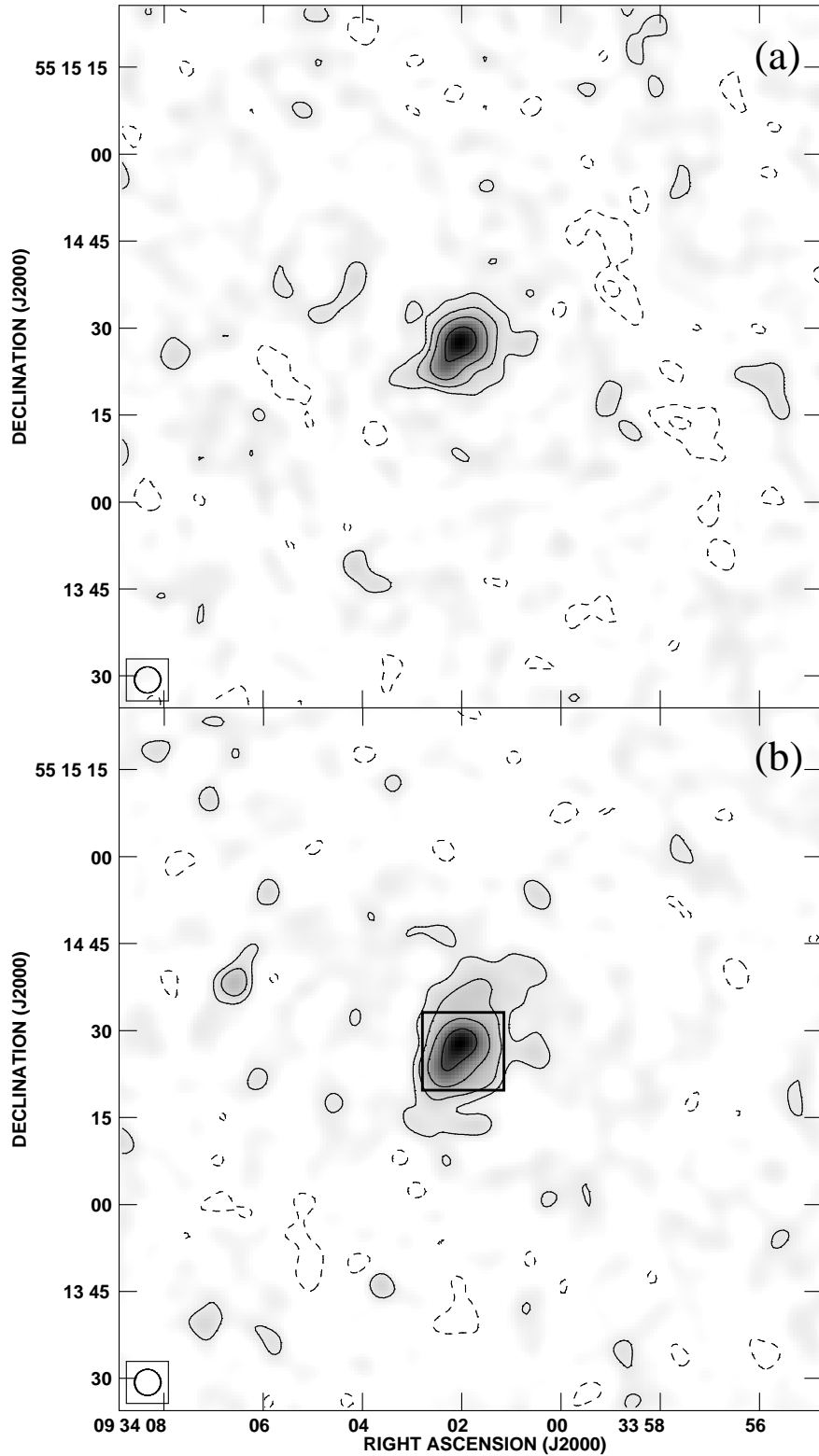


Fig. 1.— Low-resolution X-band (a) and L-Band (b) images of IZw 18, overlaid with contours at the $(-4, -2, 2, 4, 8, 16)\sigma$ levels (X-band $1\sigma = 12 \mu\text{Jy beam}^{-1}$; L-band $1\sigma = 19 \mu\text{Jy beam}^{-1}$). The beam size is $4.5'' \times 4.5''$ and is shown at the bottom left. The black box in (b) outlines the approximate field of view shown in Figures 2 and 3. Note that the diffuse emission is more spatially extended at 20 cm than at 3.6 cm.

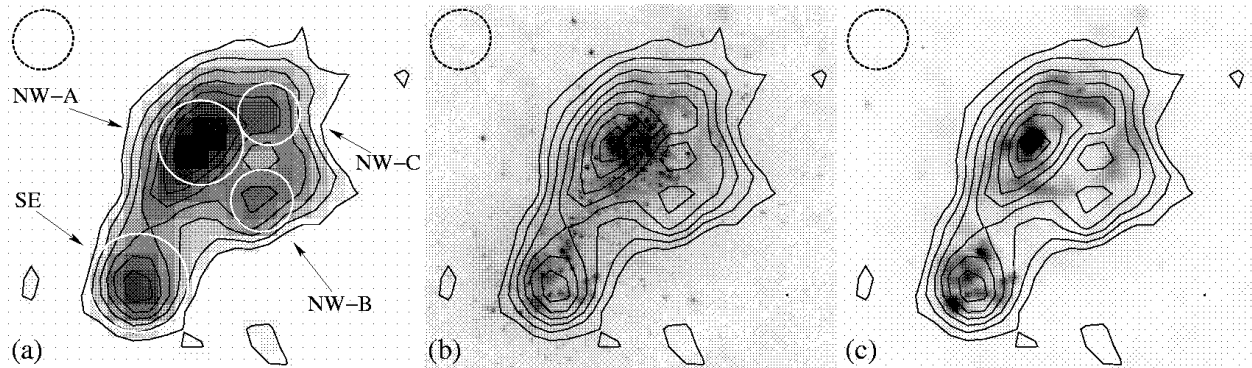


Fig. 2.— High-resolution X-Band emission contours at the -3 , 3 , 4.5 , 6 , 7.5 , 9 , 10.5 , 12 , & 13.5σ levels ($1\sigma = 7.4 \mu\text{Jy beam}^{-1}$), superposed on a grey-scale image of the emission (a), on an *HST*/ACS F555W (V) image (b), and on an *HST*/WFPC2 F656N (continuum-subtracted $\text{H}\alpha$) image (c). Labels and the white circles in (a) denote the apertures used to measure fluxes of individual peaks in the radio continuum and in $\text{H}\alpha$; see § 3 and Table 1. The beam size is $2.17'' \times 2.07''$, and is shown at upper left. The field of view (with north up and east to the left) is $\sim 0.9 \times 0.8$ kpc at the adopted distance of 12.6 Mpc.

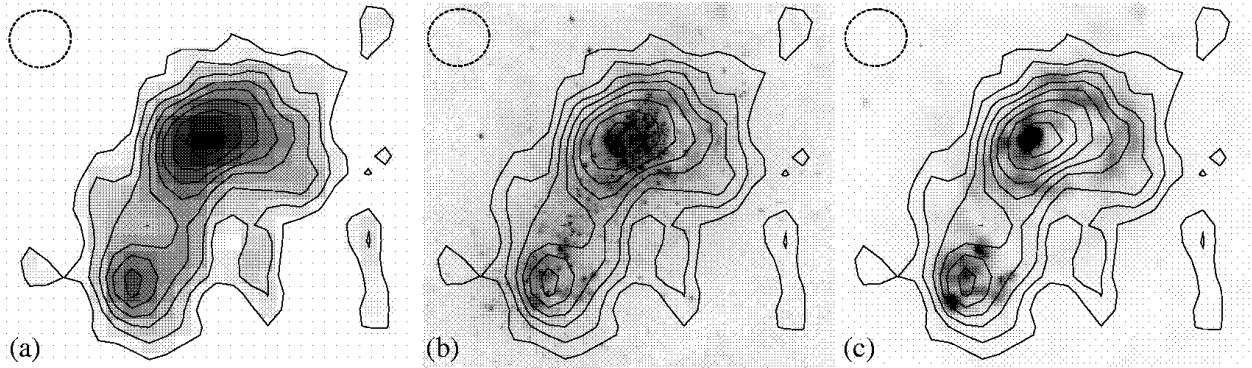


Fig. 3.— Same as Figure 2, but for the L-band high-resolution data ($1\sigma = 11.6 \mu\text{Jy beam}^{-1}$). Comparing to the X-band emission at similar resolution, it is clear that the individual emission peaks are less well-defined; we interpret this as the result of the additional synchrotron component at L-band. The beam size is $2.18'' \times 2.04''$, and is shown at upper left.

Table 1. Properties of Radio Continuum Emission in IZw 18

Parameter	IZw 18 SE ^a	IZw 18 NW-A ^a	IZw 18 NW-B ^a	IZw 18 NW-C ^a	IZw 18 Total Galaxy
R.A. (J2000) ^a	09:34:02.36	09:34:02.10	09:34:01.85	09:34:01.82	09:34:02.0
Dec. (J2000) ^a	+55:14:23.10	+55:14:28.06	+55:14:26.00	+55:14:29.06	+55:14:28
Aperture Radius (″)	1.75	1.5	1.1	1.1	—
S _L Band (mJy)	0.17 ± 0.02	0.20 ± 0.02	0.050 ± 0.005	0.079 ± 0.008	1.79 ± 0.18
S _X Band (mJy)	0.11 ± 0.01	0.12 ± 0.01	0.047 ± 0.005	0.050 ± 0.005	0.78 ± 0.08
α ($S_\nu \sim \nu^\alpha$)	-0.27 ± 0.06	-0.29 ± 0.06	-0.04 ± 0.06	-0.26 ± 0.06	-0.46 ± 0.06
H α Flux (10^{-14} erg s ⁻¹ cm ⁻²)	7.7 ± 0.8	7.8 ± 0.8	1.3 ± 0.2	2.9 ± 0.3	32.6 ± 3.3

^aSee Figure 1 for positions. The central position of radio continuum emission peaks are derived from Gaussian fitting. The coordinates of the IZw 18 system are taken from the NASA Extragalactic Database.